Master's Thesis

Fabrication of mixed-scale PMMA (polymethyl methacrylate) fluidic device via thermal nanoimprint using a convex carbon mold

Jisoo Hong

Department of Mechanical Engineering

Graduate School of UNIST

2017

1

Fabrication of mixed-scale PMMA (polymethyl methacrylate) fluidic device via thermal nanoimprint using a convex carbon mold

Jisoo Hong

Department of Mechanical Engineering

Graduate School of UNIST

Fabrication of mixed-scale PMMA (polymethyl methacrylate) fluidic device via thermal nanoimprint using a convex carbon mold

A thesis/dissertation
submitted to the Graduate School of UNIST
in partial fulfillment of the
requirements for the degree of
Master of Mechanical engineering

Jisoo Hong

1. 16. 2017

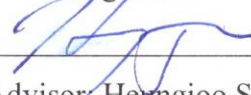Approved by

_____

Advisor

Heungjoo Shin

Fabrication of mixed-scale PMMA (polymethyl methacrylate) fluidic device via thermal nanoimprint using a convex carbon mold

Jisoo Hong

This certifies that the thesis of Jisoo Hong is approved.

01. 16. 2017

signature

_____

Advisor: Heungjoo Shin

signature

_____

Thesis Committee member: Taesung Kim

signature

_____

Thesis Committee member: Hoon Eui Jeong

signature

_____

4

Abstract

Recently micro-/nanofluidic devices are widely used for various research areas including biological, chemical, and biomedical applications. Such mixed-scale micro-/nanofluidic devices are generally fabricated using photolithography and direct writing methods (e. g., e-beam lithography or focused ion beam milling) in series. However, the direct writing methods require high cost and long process time thus resulting in low throughput issue. PDMS (Polydimethylsiloxane) replication can overcome the low throughput issues. The PDMS replication method consists of a PDMS casting process on a pre-patterned mold and a subsequent curing processes. By this method, PDMS mixed-scale channel patterns can be replicated repeatedly, thus, total throughput of fabricated mixed-scale PDMS fluidic device is enhanced. However, the channel size is smaller, the more PDMS channels are collapsed due to the low Young's modulus and hardness of PDMS.

In this study, I developed the fabrication method of mixed-scale PMMA (Poly methyl methacrylate) fluidic device via simple thermal nanoimprint using a monolithic mixed-scale convex carbon mold (microchannel mold: width = ~ 50 μm, height = ~ 5 μm; nanochannel mold: width = ~ 600 nm, height = ~ 60 nm). The monolithic carbon mold was fabricated using carbon-MEMS consisting of two step photolithography processes and one step pyrolysis. In pyrolysis, polymer structures shrank dramatically and thus microscale photoresist structures were converted into sub-micro- or nanoscale carbon structures. In nanoimprint process, the shape of the monolithic mixed-scale convex carbon mold was transferred into a PMMA sheet while the polymer sheet was heated. After demolding the carbon mold from the patterned PMMA sheet, the patterns were accurately transferred on the PMMA sheet

5

(microchannel: width = ~ 50 μm, height = ~ 5 μm; nanochannel: width = ~ 600 nm, height = ~ 60 nm).

The pyrolyzed carbon mold could be easily demolded because of its curved side walls resulting from anisotropic volume reduction in pyrolysis. This special side wall geometry and good robustness of the carbon mold ensured reproducibility in nanoimprint. The mixed-scale channels were sealed by another thin PMMA sheet with low pressure and heat after oxygen plasma treatment. PMMA has higher Young's modulus compared to PDMS (polydimethylsiloxane) so that the PMMA channels ensured consistent nanochannel fabrication and operation without channel collapse.

The PMMA mixed-scale fluidic device was used to entrap single particles via diffusiophoresis. In the fluidic device, microchannels and nanochannels were smoothly connected via Kingfisher-beak-shaped 3D microfunnels that were converted from polymer triangular prims via pyrolysis. By filling two microchannels that are connected via multiple nanochannels with high concentration solution and low concentration solution respectively and controlling pressure difference between two microchannels, local concentration gradients can occur near the 3D microfunnels at the microchannel with low concentration. The localized concentration gradients generate local electric fields resulting in diffusiophoresis; the motion of charged particles along the localized electric fields. In this experiment, 1 μm-diameter charged single particles dispersed in the low concentrate solution were dragged from the microchannel into the 3D microfunnels via diffusiophoresis. Consequently, the unique 3D microfunnel worked as a chamber where single particle was entrapped; thus, single particles could be entrapped without external electric force in 3D microfunnels. The diffusiophoresis-based single particle entrapment experiment showed the potential of the mixed-scale channel networks as a single cell research tool.

6

Dedication

I dedicate this thesis to my parents who gave me endless love with a strong trust for all my life.

And I thanks to his love, patient, kindness and support.

Without their sacrificial love, I wouldn't get this academic achievement.

List of figures

List of tables

Contents

1

Introduction

After describing conventional micro-/nanochannel fabrication methods,

the necessity of novel fabrication method is suggested

depending on the disadvantages of conventional methods.

1. Introduction

1.1 Necessity of mixed-scale fluidic device

After micro-/nanochannels were emerged in biological engineering, advanced bioanalysis applications can be possible because the micro-/nanofluidic devices have some advantages including low sample consuming, fast response time, and possibility of molecular scale analysis. Especially, the channel size is reduced to nanoscale, unique phenomena such as ion concentration polarization [1, 2], electrical double layer overlap [3], DNA stretching [4], ion rectification [5, 6], and particle filtration and separation [7, 8], and precise flux injection [9] can be shown in nanochannels which have never be seen in macro-/microscale fluidic channels. By making of use these unique phenomena, novel applications can be possible so inventive researches such as sea water desalination [10], enhancement of sensitivity for immune-sensor [11], DNA analysis [12 - 13], nanofluidic diode [14], biomolecule and particle separation [15 - 17], and nanoelectroporation [17 - 18] can be carried out in nanochannels.

Recently, contrary to a nanofluidic device having nanoscale channels only, mixed-scale fluidic device has been introduced. Mixed-scale fluidic device consists of microchannel and nanochannel simultaneously in a single fluidic chip. Since these two different scale channels are connected smoothly, the mixed-scale channels form a single channel network. This mixed-scale fluidic device is generally recommended as a promising analysis tool in bioengineering because efficient mass transport of analyte particles or molecules could be possible from bulk reservoir to extremely small location via microchannel [15, 19 - 21]. The microchannel guides particles or molecules filled in reservoir to be flowed from bulk reservoir to nanochannels. This cooperation of the different scale channels enhances manipulation of moving of particles and molecules which improves molecule accessibility into targeted

15

nanochannel location. This result contributes the mixed-scale fluidic to be primarily used in various

researches.

The more demand of mixed-scale fluidic device is increased, easy and cost-effective fabrication

methods of mixed-scale channel are required. Conventional fabrication methods are generally used

however, those have their own limitation. Here, we discuss about the fundamental conventional

fabrication methods and their limitation first. Next, we suggest the necessity of novel fabrication

methods to overcome the limitations observed in conventional fabrication methods.
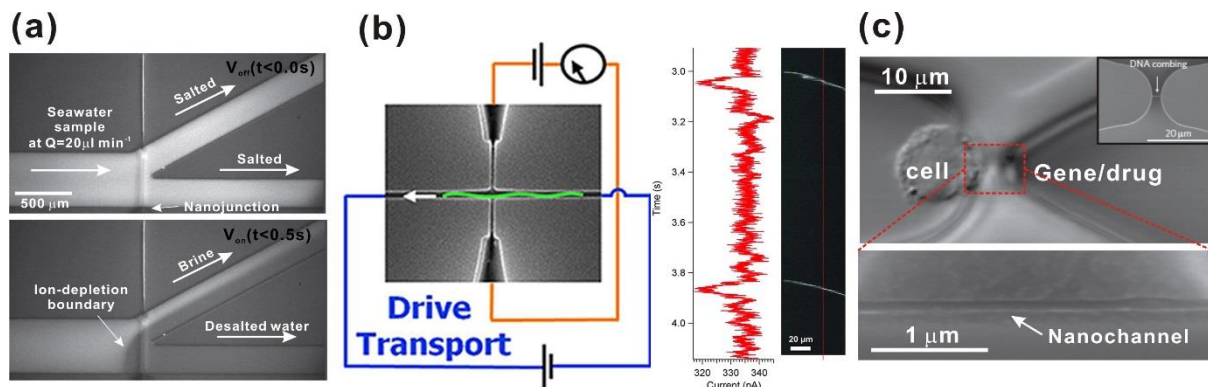
Figure 1.1 Representative nanofluidic device applications. (a) Water desalination by ion concentration polarization [10], (b) transvers ionic current measurement via translocation of stretched DNA molecules [12], and (c) nanoelectroporation via precise gene/drug injection through nanochannel [18].

1.2 Conventional fabrication methods of mixed-scale fluidic device

To fabricate mixed-scale fluidic device, standards MEMS (Micro electro mechanical systems)

techniques have been used in micro-/nanochannel fabrication. Depending on the fabrication immediacy,

these methods are categorized into two types; direct channel engraving and replication. Direct channel

engraving method is an immediate channel inscribing method on the silicon wafer or glass substrate [22

- 30]. Whereas, replication is channel pattern duplication method using a mixed-scale convex mold [31

- 40]. In this chapter, fundamental fabrication methods of direct channel engraving and replication are

explained and their strengths and weaknesses are discussed. In conclusion, the necessity of novel

method for efficient mixed-scale channel fabrication is suggested to achieve high resolution and high

throughput channel fabrication.
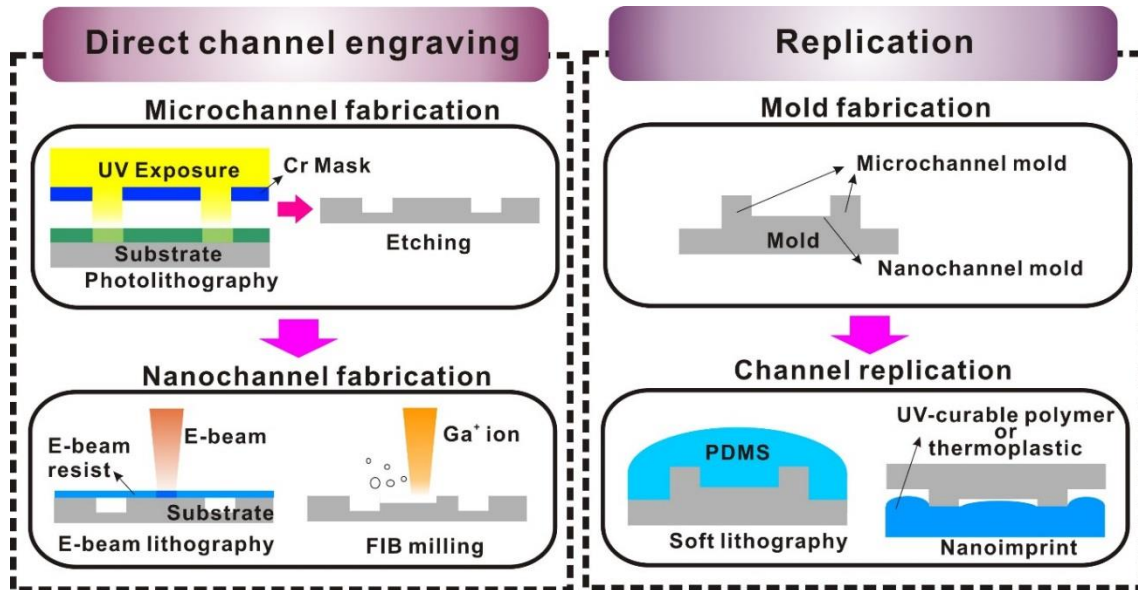
Figure 1.2 Diagram of conventional mixed-scale channel fabrication methods. Depending on the fabrication immediacy, fabrication methods are categorized into two types; direct channel engraving and replication. Direct channel engraving method consists of two different scale channel fabrication processes, sequentially. Replication is one step mixed-scale channel duplication process using a mixed-scale convex mold.

1.2.1 Direct channel engraving

In the direct channel engraving method, the micro- and nanochannel patterns are sequentially

carved on the substrate. In general, microchannel is fabricated by photolithography with etching process

[22 - 25], while, nanochannel is fabricated by direct writing method including e-beam lithography [26

- 27] and focused ion beam milling process [28 - 30].

Photolithography is the most common method for patterning polymer structures. On the silicon

substrate, liquid-state photoresist polymer is spin-coated. Photoresist is UV reactive material so photoresist solubility can be changed through UV exposure. To make a polymer pattern, the spin-coated photoresist is exposed to UV through the photomask, then, UV exposed/non-exposed parts of photoresist are cured depending on the opened/non-opened photomask pattern because photomask is designed by transparent and opaque chrome region. After UV exposure process, the soluble parts of photoresist are removed while non-soluble polymers remain completing polymer structure. These patterned polymers cover specific substrate regions, whereas, other parts of substrate are non-covered. Then, the non-covered regions of substrate are etched by subsequent etching process such as wet etching or dry etching, lastly microchannel patterns are carved on the substrate. Because the photolithography is simple and well-established methods these were often used in microchannel fabrication. In addition, by changing photomask design and manipulating etching rate, various shapes and depth of channel control are also feasible. However, in terms of pattern resolution, the size of channel width can't be reduced under 1 μm because UV is diffracted at the edge of the photomask pattern interrupting high resolution. This result restricts photolithography to be used in nanochannel fabrication.

The limitation of resolution can be overcome by direct writing techniques including electron beam (e-beam) lithography (EBL) and focused ion beam (FIB) milling. Through the highly intensive e-beam or focused ion beam, nanoscale channels are directly written on the substrate due to the extremely small diameter of electron or focused ion beam. The different thing between two techniques, e-beam lithography is commonly used in polymer patterning so it needs subsequent etching process for concave nanochannel fabrication. After spin coating e-beam resist on the substrate, e-beam draws long and narrow line patterns on the e-beam resist. Then solubility of e-beam resist is changed and

nanochannel patterns are formed by open/covered e-beam resist parts. By subsequent etching process,

open regions of substrate are engraved which are converted into concave nanochannels. Contrastively,

focused ion beam can directly carve nanochannels, so, it doesn't need resist layer and subsequent

etching process.

From those direct writing methods, nanochannels can be fabricated successfully, however,

direct writing method is expensive, low throughput and time-consuming process. Therefore, it reduces

total throughput of fluidic channels fabrication. In addition, in terms of sequential process, the precise

alignment process of microchannel and nanochannel should be carried out for well-interconnected

channel networks because two different scale channels are carved individually through two step

processes. Therefore, one step channel network fabrication method with high throughput is required

and this is solved by replication method.
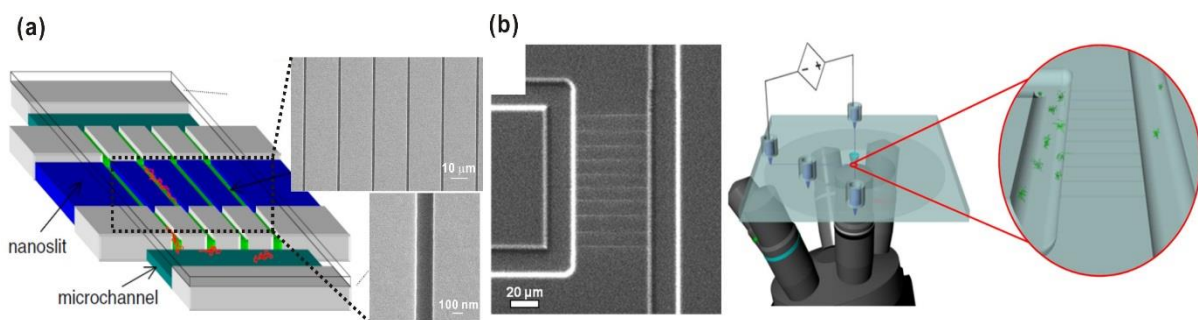
Figure 1.3 Mixed-scale channel were fabricated on the glass substrate via direct engraving channel fabrication method. (a) Schematic of mixed-scale fluidic device with DNA stretching (left) and scanning electron microscope (SEM) image of nanochannels (right). Nanochannels were fabricated by e-beam lithography with etching [25]. (b) SEM images of mixed-scale channel patterns (left). The nanochannels were fabricated by focused ion beam milling process [30]. Microchannels were fabricated by photolithography with etching in (a) and (b).

1.2.2 Replication

Replication can overcome the limitations of the direct engraving methods in terms of process

cost and time. Basically, replication is performed by duplication of engraved patterns from concave

mold structures. Owing to the reusability of mold, plenty of same fluidic channels patterns can be

transferred from one mold, repeatedly. This reproducibility results in high throughput fabrication which

was not available in direct engraving methods. In addition, because the mold having both two different

scale convex structures, mixed-scale channels are simultaneously transferred by only one step

replications. Therefore, replication method is much more efficient than direct engraving method to

produce fluidic channels and it is well-applied in the all-round fluidic device fabrication.

PDMS (polydimethylsiloxane) channel replication via soft lithography is the most

representative method in fluidic device fabrication [31 – 35]. After preparing a pre-patterned convex

mold with mixed-scale structures, liquid-state PDMS is poured on the convex mold. The PDMS is

generally mixed with curing agent at a ratio of 10 to 1, respectively. The liquid-state PDMS is cured

into a solid mass at 75 ~ 80 °C temperature for 3 hours. Then, the cured and mixed-scale channel

patterned PDMS is detached from the mold. After sealing the transferred PDMA channels with thin

cover glass after oxygen plasma treatment, this completed PDMS chip is used as a fluidic device itself.

Even though the simple fabrication process of PDMS fluidic device, PDMS is unsuitable material for

nanofluidic chips because the channel size becomes to nanoscale, PDMS channels easily collapse due

to the low hardness and Young's modulus of PDMS specially during channel sealing process. To escape

the channel collapse, relatively hard-PDMS layer should be added on the general PDMS mass surface,

20

but it is not a perfect resolution and it just supplements inconvenient fabrication process. In addition, PDMS curing time is at least 2 ~ 3 hours which is long process time.

As another replication, the importance of nanoimprint has been risen because the materials used in nanoimprint replication can make up for the material weakness of PDMS. Comparing with PDMS replication, nanoimprint uses relatively hard materials such as UV-curable polymer or thermoplastic for fluidic device. These are more durable than PDMS, so even though the channel size is reduced up to nanoscale [36 - 40], these channels are not collapsed. And nanoimprint process need relatively short process time comparing with PDMS curing, therefore, it is more suitable for high productive fabrication method. Depending on the type of resists, nanoimprint methods are classified into two types; thermal nanoimprint and UV nanoimprint. Thermal nanoimprint uses thermoplastic and the other UV nanoimprint method uses UV-curable polymer.

First, in thermal nanoimprint, originally solid state thermoplastic is changed into quasi-liquid state at high temperature above its glass transition temperature. Then, a convex monolithic mold is put on the thermoplastic surfaces and pressed down with high pressure to imprint concave mold structures. During imprinting, quasi-liquid state thermoplastic is deformed while filling the mold cavities - concave parts of the mold, then, opposite morphology of the mold is duplicated on the thermoplastic. After imprinting, the deformed thermoplastic is re-solidified with cooling under high compression and it can be detached from the mold. In this case, commercialized thermoplastic sheets are often used such as PMMA (polymethyl methacrylate) or PC(polycarbonate) because these materials are easy to buy at markets and easily deformable via thermal nanoimprint method. Whereas, in UV nanoimprint, a liquid

state UV-curable polymer is spin-coated on the substrate. Then, the mold is put on the polymer layer and pressed down to be filled with UV-curable polymer in mold cavities. Because the UV-curable polymer has low viscosity, it needs relatively low pressure comparing with thermal nanoimprint process. After filling mold cavities, UV light is exposed to liquid-state polymer layer to be changed into solid-state. As the same method with thermal nanoimprint process, the mold and resist layer are detached after curing polymer and solidified polymer with channel patterns is sealed for completing fluidic device fabrication.

The most critical issue in nanoimprint is it requires mechanical contact process with high pressure since the accuracy of transferred channel patterns is dependent on the how much mold cavities are clearly filled with the polymer resist. Therefore, it is depending on the pressure strength and polymer viscosity. However, in high pressure state, convex mold structure is easily damaged, specially, in case of nanostructures. In case of thermoplastic, its viscosity is reduced at high temperature, however, it is still quasi-liquid state. And the high temperature causes mold damage due to thermal expansion difference between mold and polymer which bothers demolding after cooling. To escape thermal and pressure damage, UV-curable polymer is used because it is liquid-state material, therefore, imprinting pressure and heating temperature is lower than thermal nanoimprint process. But UV-curable polymer certainly needs transparent mold or substrate for being exposed to UV which are fabricated by expensive materials and complicate manufacturing process.

Above those limitations, all replication methods still have convex mold fabrication problem to achieve one step mixed-scale channel replication because the convex nanostructure fabrication still needs inconvenient direct writing methods. As an alternative for mold fabrication, replica mold has been introduced. Replica mold is a duplicated convex polymer structure from engraved channel structure. After mixed-scale channel fabrication via direct engraving method, several replica molds can be replicated from the mixed-scale channel structure which is called master mold. Because plenty of replica molds can be fabricated from one master mold, the total throughput is increased. However, transferring accuracy of pattern is decreased due to two step replication process. This error is not significant in microchannels but for nanochannels [35, 37].
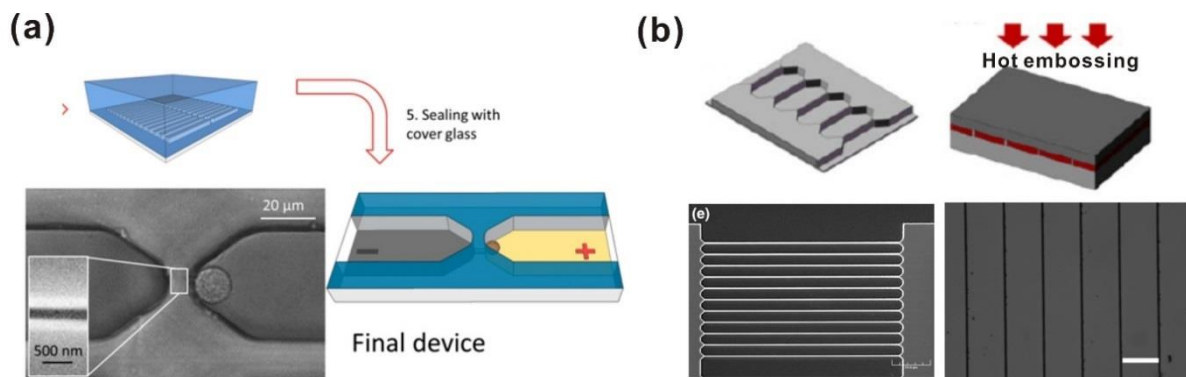
Figure 1.4 Mixed-scale channel fabrication by replication. (a) Schematic of PDMS channel fabrication (right) and SEM image of completed mixed-scale channel (left) [29]. (b) Schematic of nanoimprint fabrication (upper) and SEM images (bottom) of mixed-scale silicon mold for nanoimprint (left) and corresponding transferred nanochannel via nanoimprint (right) [38].

1.3 Novel fabrication method of mixed-scale fluidic device

1.3.1 Carbon-MEMS

As a versatile wafer-level microfabrication technology, carbon-MEMS (C-MEMS) technology has been utilized for fabricating convex micro- or mixed-scale carbon molds. The carbon-MEMS is

manufacturing technique of carbon structure. Carbon-MEMS process consists of two main fabrication steps. First step is building of polymer precursor and second step is converting the polymer precursor into carbon structures. Once polymer structures are established as precursors, the polymer precursors can be decomposed slowly at high temperature in no oxygen environment. This decomposition is called pyrolysis and the pyrolyzed polymers are converted into carbon structures with large volume shrinkage. Even the volume reduction is up to 90%, original frame of polymer precursor is not changed. Thus, owing to the carbon-MEMS, complex carbon structure can be easily fabricated via only polymer patterning process before pyrolysis without direct carbon shaving process.

Representatively, photolithography and nanoimprint are generally used as polymer patterning techniques. For example, photoresist is commonly used as the polymer precursor material because photoresist can be patterned depending on photomask design and spin-coated photoresist thickness. This makes it possible not only for simple fabrication of complex and high aspect ratio convex carbon structures but also micro-/nanoscale carbon structure fabrication such as high-aspect-ratio cylinder arrays [41] nanoelectrode arrays [42] and suspended nanowires [43 - 44]. Those complex carbon structures are used as an electrode for various electrochemical sensors.

Except for those conventional used places of carbon, the novel availability of the pyrolyzed carbon as a mold can be discussed. The potential of carbon mold was already demonstrated in previously published papers. Youn *et al*. demonstrated that glassy carbon is a good candidate for a mold material because it has favorable properties such as low surface energy, chemical stability, high hardness, high wear resistance, and gas impermeability [45 – 46]. Especially high durability of carbon material at high temperature facilitated efficient glass channel fabrication using hot embossing process repeatedly. But

the convex glassy carbon mold was fabricated by direct etching process on the glassy carbon substrate, so fabrication process was not simple. Whereas, Ju *et al.* introduced a convex pyrolyzed carbon mold which was converted from a furan-based thermal curable polymer precursor and this structure was patterned via soft-lithography [47]. This carbon mold consisted of convex microscale line structures. So, it engraved concave line patterns on the glass substrate at high temperature with high pressure. Even the glass imprinting process needed over 600 °C temperature, the glassy carbon mold could tolerate harsh glass channel imprinting process because the pyrolyzed carbon mold was formed at much higher temperature up to ~ 1000 °C.

Recently, Lee *et al.* introduced a mixed-scale fluidic device fabrication using a pyrolyzed monolithic mixed-scale convex carbon mold [17]. This mold could be made by maximizing volume reduction during pyrolysis which was up to ~90%. From this method, convex carbon nanostructures (width ~ 720 nm, height ~ 32 nm) could be simply fabricated at a wafer level from microscale photoresist precursors (width ~ 1.1 μm, height ~ 210 nm) which were patterned using conventional photolithography without any complex and expensive nanofabrication technologies. In addition, to make a monolithic mixed-scale convex carbon mold, additional photoresist patterning process was added for microchannel mold structures. After small photoresist patterning (width ~ 1.1 μm, height ~ 210 nm), large photoresist patterning (width ~ 100 μm, height ~ 25 μm) was be added, thus, the two-different photoresist structure formed a monolithic polymer precursor and after pyrolysis, a monolithic mixed-scale mold fabrication was completed. Using the monolithic convex mold, mixed-scale PDMS channel networks was simply replicated and the replicated channel networks could be completed with a cover glasses via oxygen plasma assisted covalent bonding. Specific point of the mixed-scale carbon

25

mold was utilizing anisotropic volume reduction of polymers in pyrolysis. Because the polymer

structure was adhered to the substrate, upper part of the polymer shrunk more than the bottom part, thus,

vertical polymer side walls were converted into inclined carbon side walls. This inclined side walls

contributed to efficient demolding with relatively low surface energy of the pyrolyzed carbon structures.

As described in this chapter, it can be expected that the most critical issues of conventional

channel fabrication method can be overcome by the mixed-scale monolithic convex mold composed of

mechanically and chemically strong glassy carbon fabricated by carbon-MEMS technique. This mold

satisfies crucial requirements for cost-effective mixed-scale mold fabrication through microfabrication

methods only and alleviate difficult accurate alignment of two different scale channel patterns. It can

also endure several harsh replication processes owing to the mechanical and chemical properties of

carbon. Therefore, in this paper, carbon mold is used as a mixed-scale channel mold in thermal

nanoimprint process and the superior availability is demonstrated in next chapter.
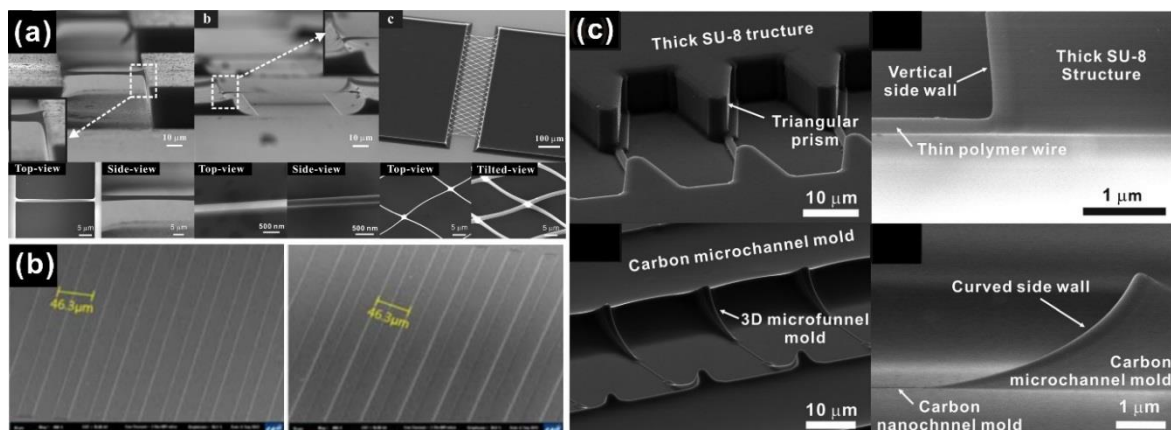
Figure 1.5 SEM images of carbon structure via pyrolysis. (a) Suspended carbon nanowire and carbon mesh structures [42]. (b) Pyrolyzed microchannel carbon mold (left) and corresponding glass microchannels transferred by hot embossing (right) [47]. (c) Mixed-scale pyrolyzed carbon mold with convex structure. SU-8 (upper) structures were converted to carbon structure (bottom). Vertical SU-8 side wall was changed into inclined carbon side wall [17].

1.3.2 Thermal nanoimprint

In accordance with the reduced size of channel, productive replication with non-collapsed material is required to replace PDMS. In company with the requirement, properly corresponded fabrication method has been developed.

Thermal nanoimprint is efficient way to alternate PDMS channels in terms of material properties. In comparing with PDMS, thermoplastic has relatively high Young's modulus and hardness so thermoplastic channels are not to be easily collapsed even channel size is becoming smaller. Furthermore, nanoimprint is also included in replication so that it can keep the high productivity of fluidic channels fabrication. Besides, thermoplastic is easily heated and deformed, process time is also shorter than PDMS process. Above those advantages, thermal plastic is transparent, manageable, and easy to buy in common market so it is more practicable in biological analysis research. Several research teams already tried to fabricate thermoplastic fluidic devices. Also, those were successfully utilized in biological applications. [48 - 49].

In fact, UV nanoimprint method is more beneficial than thermal nanoimprint in terms of mold durability due to non-harsh imprinting conditions with low pressure and low temperature. Further, UV-curable polymer is liquid state so it is profitable for exact duplication of channel patterns since liquid more easily fills mold cavities than viscoelastic state thermoplastic at high temperature. Despites of the advantages of UV nanoimprint, here, thermal nanoimprint method is recommended more than UV nanoimprint since UV nanoimprint has other limitations; UV nanoimprint must need transparent mold or transparent substrate. Because it is originally liquid-state so it should be spin-coated on the substrate.

And it is essential for UV-curable polymer to be solidified via being exposed to UV light. Therefore, transparent glass or quartz are used for mold and substrate, but these are expensive material and need difficult manufacturing process. On the other hand, thermoplastic is commercialized as a sheet form having various thickness from hundreds of micrometers to number of millimeters, so, it is more feasible to handle in imprinting process directly. Besides, thermoplastic is not expensive and easily deformed. If a mixed-scale convex mold is robust enough in thermal nanoimprinting process, thermoplastic is a good alternative to PDMS.

In this research, mixed-scale pyrolyzed carbon mold is used to thermal nanoimprint process. During nanoimprint process, this mold transferred channel patterns more than 40 times on the PMMA sheets without mold damages. From this results, it is demonstrated that the limitations of mold in thermal nanoimprint can be overcome and this fabrication method will be able to replace the prevalent PDMA fluidic device replication method.
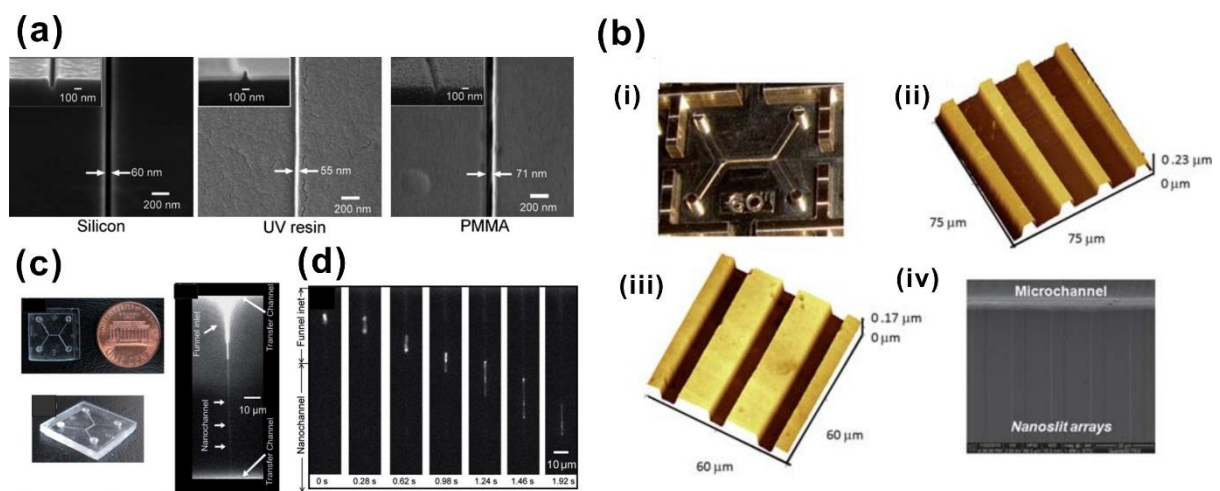
Figure 1.6 Via thermal nanoimprint process, mixed-scale channel was fabricated on the PMMA sheet. (a), (c) and (d) are referred from Wu *et al*. [47] and (b) are referred from Chantiwas *et al*. [49]. (a) SEM images of nanochannel master mold, replica mold and transferred nanochannel. (b) (i) Completed fluidic device. (ii) and (iii) are 3D AFM images of replica mold and transferred nanoslit patterns. (iv) SEM image of mixed-scale channel network. (c) Completed PMMA fluidic devices can be applied in (d) DNA stretching.

28

1.4 Thesis outline

Here, we present a novel fabrication method of mixed-scale channel networks based on a single nanoimprint process to replicate mixed-scale channel networks on a PMMA sheet using a convex mixed-scale carbon mold. The convex mixed-scale carbon mold is fabricated using only a batch microfabrication method, that is carbon-MEMS. After sealing the replicated mixed-scale PMMA channels with a thin PMMA sheet via oxygen plasma assisted thermal bonding, mixed-scale fluidic device can be completed. This fluidic device is applied in single particle entrapment experiment. A single particle is dragged smoothly into and entrapped in a Kingfisher-beak-shaped 3D microfunnel via diffusiophoresis where localized solute gradient exists. This result demonstrates a structural usefulness of 3D microfunnels for localizing solute gradient and a validity of diffusiophoresis as a principle of single cell entrapment.

2

Fabrication

To achieve thermoplastic mixed-scale channel fabrication,

pyrolyzed carbon mold, thermal nanoimprint and

oxygen plasma assisted bonding methods are explained.

2. Fabrication

2.1 Overview of mixed-scale fluidic device fabrication

In this research, micro- and nano- mixed-scale fluidic device is fabricated via two step processes; mold fabrication and channel replication. To accomplish simple one step replication, a mold should contain micro- and nano- mixed-scale monolithic convex structures. Carbon-MEMS technique facilitates the combined-scale structure fabrication using only cost-effective microfabrication methods. After mold fabrication, the monolithic carbon mold is used in channel replication via thermal nanoimprint process on the PMMA surfaces several times. The engraved channels are clearly sealed with thin PMMA sheet via oxygen plasma assisted thermal bonding process. This completed fluidic device has hydrophilicity surface and is applied in single particle entrapment experiment using diffusiophoresis.

2.2 A monolithic mixed-scale convex carbon mold fabrication – Carbon MEMS

A mixed-scale monolithic convex carbon mold is fabricated via two step photolithography and batch pyrolysis process. UV exposure is conducted by mask aligner (MA-6, Suss Microtech.) in UCRF.

First, SU-8 2000.5 photoresist is spin-coated on the 6-in silicon wafer in three steps (500 rpm 5 s, 3000 rpm 30 s, 500 rpm 3 s), then, 400 nm-thick SU-8 layer is coated on the Si wafer. This coated wafer undergoes soft baking process on the hot plate at 98 °C for 1 min and 30 seconds. After cooling the wafer until room temperature, this SU-8 wafer is firstly exposed to UV light with 40 mJ/cm^2 intensity

31

with vacuum contact through nanochannel photomask. The first UV exposure is for building 1 μm-width and 420 nm-thick small-scale polymer line patterns. Then, the exposed wafer is undergone post exposure baking process at 98 °C for 45 seconds. After cooling the wafer until room temperature again, which is developed in SU-8 developer for 1 min. By rinsing the developed wafer by acetone, isopropyl alcohol, and DI water and dry by N_2 gun, small-scale polymer precursor fabrication is finished. Second photolithography is for building large-scale polymer precursor. Before to start second photolithography, the small-scale SU-8 patterned wafer should be clearly dried. And then SU-8 2025 photoresist can be spin-coated on the Si wafer (500 rpm 5 s, 3000 rpm 30 s, 4000 rpm 5 s, 500 rpm 5 s). After spin-coating, the SU-8 2025 is layered on the wafer with 25 μm thickness and is put on the hot plate at 98 °C for 4 min for soft baking. After cooling the wafer under room temperature, this photoresist layer is exposed to UV light with 150 mJ/cm^2 intensity in hard contact through microchannel photomask. Then, the exposed wafer is put hot plate again to post exposure baking process at 98 °C for 5 mins. If the wafer is cool down enough, it can be also developed in SU-8 developer. Then, the patterned large-scale SU-8 precursor having 100 μm-width and 25 μm-thick lines and triangular prism are added resulting in a monolithic polymer precursor structure.

This monolithic SU-8 structure should pass through pyrolysis process in the tube furnace at a high vacuum condition. The internal pressure is stable under 10^{-3} torr and the temperature of furnace is increased up to 900°C with 1°C increasing /1 min. Then, the SU-8 structure starts to be pyrolyzed and converted into monolithic convex carbon mold with mixed-scale mold structures. This mixed-scale carbon mold is composed of ~ 600 nm-width and ~ 60 nm-height nanochannel mold and ~ 50 μm-width and 5 ~ 6 μm-height microchannel mold with Kingfisher-beak-shaped 3D structure. After pyrolysis and cooling down tube furnace, the mold is un-loaded. The all steps of mold fabrication are described in figure 2.1.
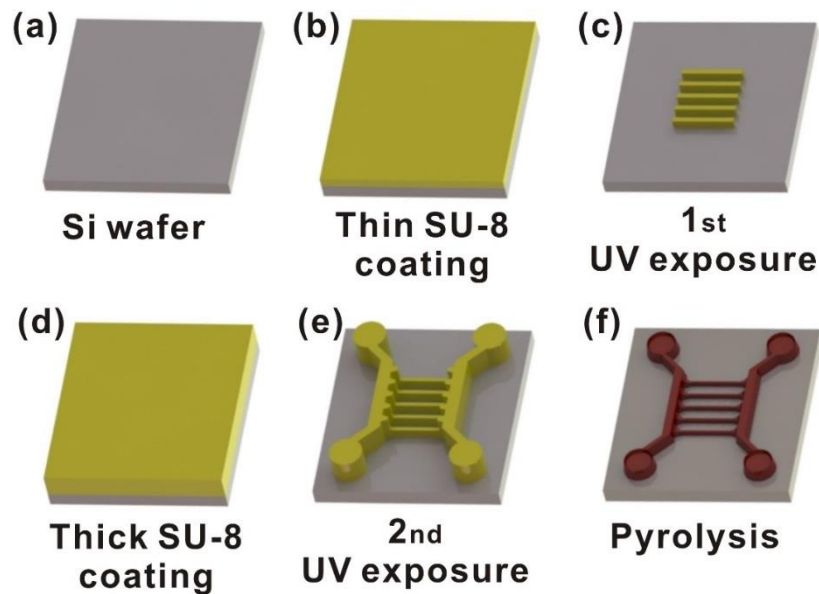
Figure 2.1 Schematic of a mixed-scale monolithic convex carbon mold fabrication.

2.3 One step mixed-scale channel replication and sealing

– Thermal nanoimprint and oxygen plasma assisted thermal bonding

Using the mixed-scale convex carbon mold, channel patterns are transferred on the PMMA sheet

via one step thermal nanoimprinting. The thermal nanoimprint machine is order-made facility. This machine contains main chamber with 4-in main chuck, quartz roof, load cell and heater. And the internal pressure of main chamber can be manipulated by oil pump so the pressure gauge can be reduced under 10^{-2} torr. Heater is set under main chuck so it heats bottom surface. By air pressure, main chuck is moved up, then, quartz roof and main chuck are contacted and pressed. This pressure gauge is measure by load cell set under main chuck which is increased up to 250 kg.

First, bare silicon wafer is put on the main chuck and carbon mold is put on the bare silicon wafer. Then, 3 mm-thick and 5 cm-width $\times$ 5 cm-length PMMA sheet is put on the carbon mold. And wait the main chuck is heated until 130 °C for 5 min. Because the heater is placed under chuck, the temperature is increased from bottom PMMA sheet to top PMMA surface. During heating, the main chamber pressure is decreased under 5×10^{-2} torr. When the vacuum gauge and chuck temperature are stable, the chuck is pressed up to quartz roof so both main chuck and quartz roof press the carbon mold and PMMA sheet simultaneously with 2 ~ 3 MPa pressure. At this condition, wait for 10 min to replicate patterns. Then, clearly mixed-scale channel networks are transferred on the PMMA sheet. The transferred microchannel has ~ 50 μm-width and ~ 5 ~ 6 μm-depth, and nanochannel has ~ 600 nm-width and ~ 60 nm-depth. Kingfisher-beak-shaped 3D structure engraves 3D microfunnel at the same time. The patterned PMMA sheet is cut into 1.5 cm-width and 1.8 cm-long individual chips with 4-mm diameter cut circle reservoirs using laser cutter (PLS 6.75, Sejoong, Korea).

The piece of patterned PMMA piece is sealed with a 175 μm-thick PMMA sheet by oxygen plasma

treatment assisted thermal bonding under glass transition temperature. Oxygen plasma treatment is

conducted in COVANCE (Femtoscience, Korea) equipment in 80W for 1 min with 15 sccm oxygen

gas injection. Owing to the oxygen plasma treatment, hydrophobic PMMA surface is changed into

hydrophilic state. Then, these two PMMA sheets are put inside thermal nanoimprint chamber again,

and pressed with 0.2 MPa at 75 °C for 4 min to be bonded. Conclusively, a mixed-scale fluidic device

is completed with leakage-free, no channel collapsed and hydrophilic surface.
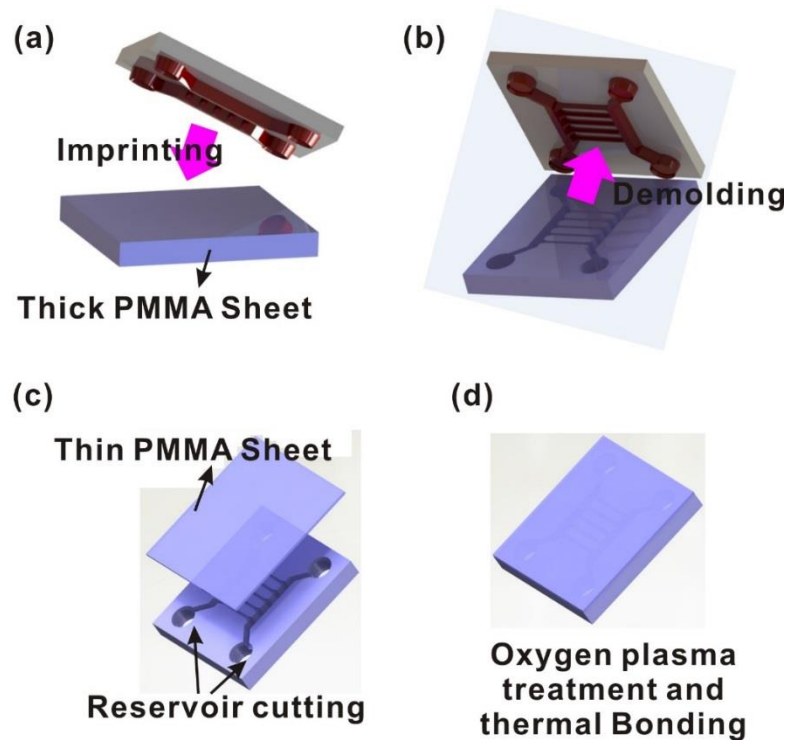
Figure 2.2 (a) Schematic of a mixed-scale channel replication via thermal nanoimprint using mixed-scale carbon mold.

3

Results

In this chapter,

the fabricated carbon mold, engraved PMMA channels and

sealed PMMA fluidic device are shown.

3. Results

2.3 Characterization of carbon mold

2.3.1 Pyrolyzed carbon morphology

A monolithic SU-8 structure was converted into mixed-scale convex carbon mold (Fig. 3.1). Owing to the two step photolithography processes, two different scale polymers formed a monolithic SU-8 structure (Fig. 3.1 (a), (b)). After pyrolysis, the monolithic SU-8 was converted into monolithic carbon structure (Fig. 3.1 (c), (d)). Since pyrolyzed carbon morphology was originated from a monolithic SU-8 structure, it also had a monolithic convex structure (Fig. 3.1. (c), (d)). Originally, the large-scale convex SU-8 had 100 μm-width and 25 μm-height structure. And it was reduced 50 μm-width and 5 ~ 6 μm-height carbon structure. Those images were taken by scanning electron microscope (S-4800, Hitachi high-technologies, Japan).

SU-8 structure had originally vertical side wall (Fig. 3.2 (a), (b)). After pyrolysis, carbon side wall was changed into inclined (Fig. 3.2 (c), (d)) form. The profile change of wall resulted from anisotropic pyrolysis of SU-8 structure because the bottom of SU-8 was on the Si substrate and adhered strongly, while top surface of SU-8 was opened to outside. Therefore, the pyrolysis rate of SU-8 was different between top and bottom so top surfaces of SU-8 were more pyrolyzed than bottom surface. This tendency helped SU-8 triangular polymer prism to be changed into Kingfisher-beak-shaped 3D carbon structure placed between micro- and nanostructure vertically (Fig. 3.1 (b), (d)). The Kingfisher-beak-shaped 3D carbon structure assisted to align microscale carbon and nanoscale carbon structure without

precise alignment process. This 3D carbon structure engraved 3D microfunnel on the PMMA sheet

which is applied to single particle entrapment as a chamber where solute gradient exists.
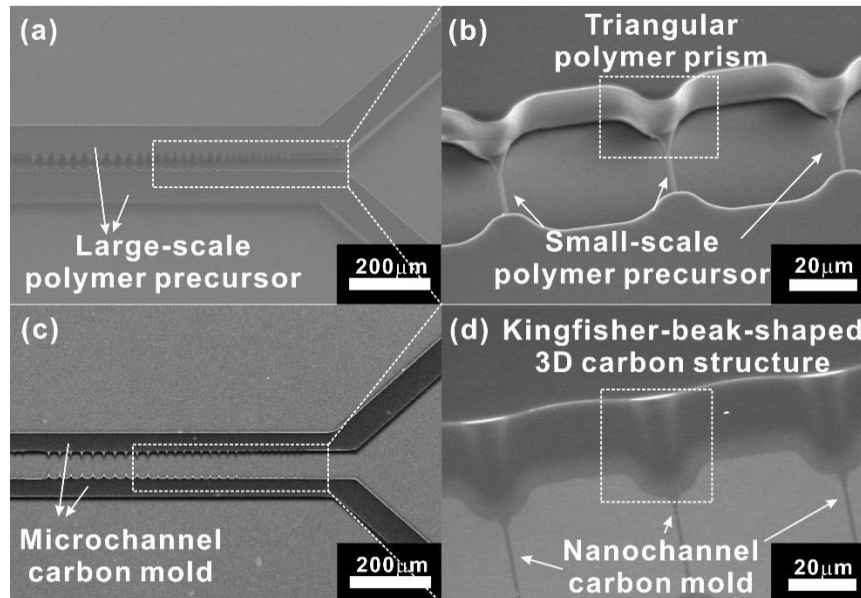
Figure 3.1 Scanning electron microscope (SEM) images of (a, b) monolithic SU-8 structure and (c, d) monolithic mixed-scale convex carbon mold. (b) Two different scale polymer precursors are vertically connected via triangular polymer. This triangular polymer prism was converted into (d) Kingfisher-beak-shaped 3D carbon structure. The 3D carbon structure helped well aligned mixed-scale carbon structure without precise alignment process.
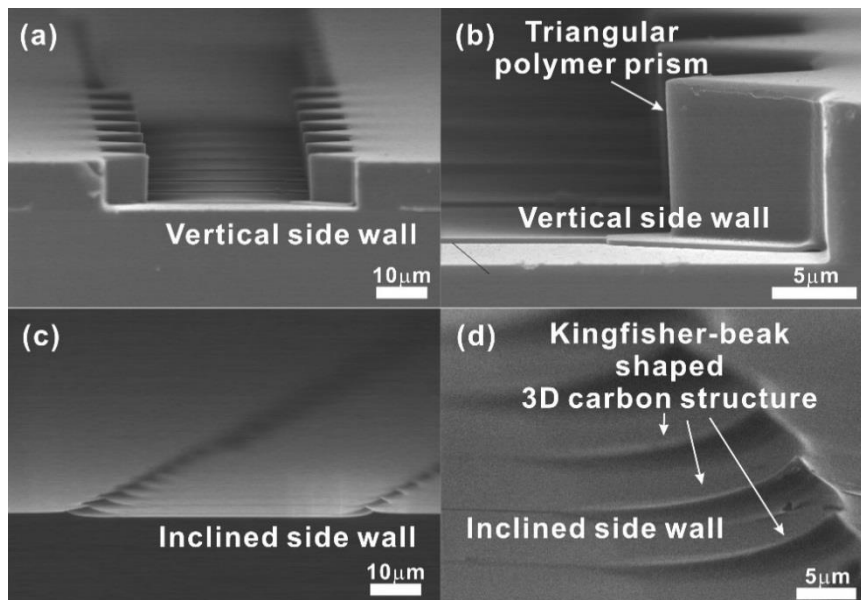
Figure 3.2 SEM images of SU-8 structure and pyrolyzed carbon structure. (a, b) Vertical SU-8 structures were converted into (c, d) Inclined carbon structures due to different pyrolysis rate between top and bottom, which resulted in Kingfisher-beak-shaped 3D carbon structure.

2.3.2 Durability and reusability of carbon mold

To demonstrate the reusability of carbon mold, several times of thermal nanoimprint processes for channel replication were carried out. We used the same carbon mold in 40 times thermal nanoimprint process. The nanoimprint process was conducted at 130 °C temperature with 3MPa pressure for 10 min. After 40 times nanoimprint, the morphology of carbon was checked by SEM images. In figure 3.3, the used mixed-scale carbon mold was not damage but there was a little contamination (Fig. 3.3 (b)). This results is more efficient than replica molds which is reused about a dozen.

To analyze mechanical properties of carbon mold, Young's modulus and hardness of SU-8 structure and pyrolyzed carbon were measured by nanoindentation. As shown in figure 3.4, Young's modulus and hardness of SU-8 were dramatically increased about 5 times and 10 times, each. Even if the measured value was much lower than silicon (Table 3.1), it is larger than PUA (polyurethane acrylate) which is a common material of replica mold. And the pyrolyzed carbon has both a little flexibility and hardness, carbon mold can endure harsh imprinting and be flexibly demolded. Therefore, it can be suggested as a promising mold.
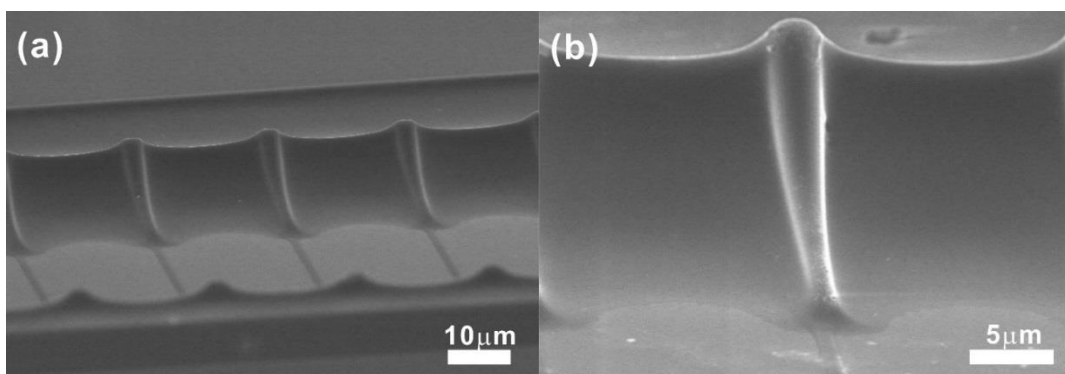
Figure 3.3 Even after 40 times thermal nanoimprint process, mixed-scale carbon mold was not damaged. (a) SEM image of mixed-scale carbon mold structure and (b) magnified Kingfisher-beak-shaped 3D carbon structure. The used mixed-scale carbon mold was not damage but there was a little contamination.
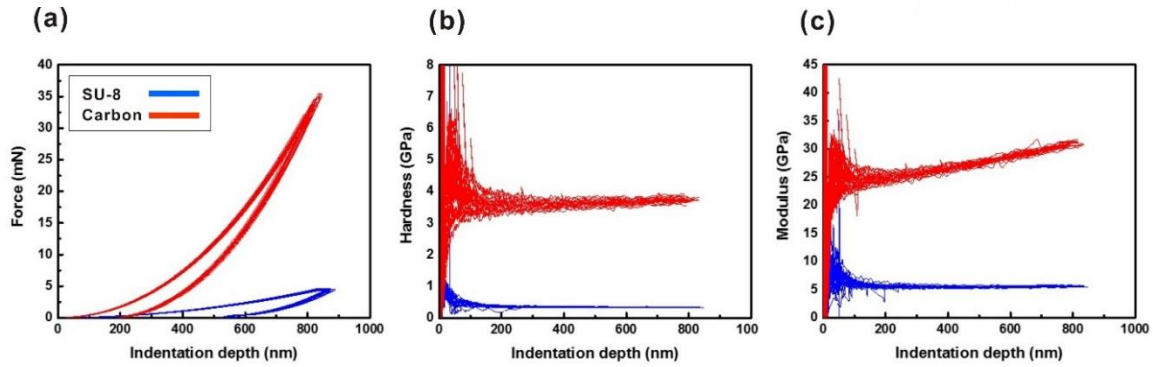
Figure 3.4. Nanoindentation measurements of SU-8 structures and pyrolyzed carbon. (a) input force for measuring, (b) hardness of SU-8 and pyrolyzed carbon and (c) Young's modulus of SU-8 and pyrolyzed carbon.

	SU-8 (measurement)	Carbon (measurement)	Silicon (reference - wiki)	PUA (reference-journal)
Young's modulus(GPa)	5.5 ± 0.1	28.8 ± 0.4	130 - 188	2.7
Hardness (GPa)	0.35 ± 0.01	3.67 ± 0.07	10.2	0.15

Table 3.1. Nanoindentation measurements of SU-8 structures and pyrolyzed carbon. After pyrolysis, Young's modulus and hardness were dramatically increased. Comparing with silicon, Young's modulus and hardness is small, but it is larger than PUA (polyurethane acrylate) which is used as a replica mold.

3.2 Characterization of PMMA (polymethyl methacrylate) channels

3.2.1 Transferred micro-/nanochannel morphology

After thermal nanoimprint, mixed-scale channel networks were successfully transferred on the

PMMA sheet. The PMMA channel patterns can be seen in figure. 3.5 comparing with carbon mold. The

convex mixed-scale carbon mold with 3D Kingfisher-beak-shaped 3D carbon structure is seen in figure

3.5 (a) and transferred concave PMMA channel network is seen in figure 3.5 (b). As shown in the figure,

the mixed-scale patterns were accurately transferred on the PMMA sheet. In figure 3.6 (a), Kingfisher-

40

beak-shaped 3D carbon structure connected microchannel mold to nanochannel mold vertically. This

3D carbon structure was transferred on the PMMA resulting in Kingfisher-beak-shaped 3D microfunnel

(Fig. 3.6 (b)). Through the 3D microfunnel, the deep and large horizontal microchannel was connected

to nanochannel vertically and smoothly because the cross section of 3D microfunnel is gradually

reduced to nanochannel size.
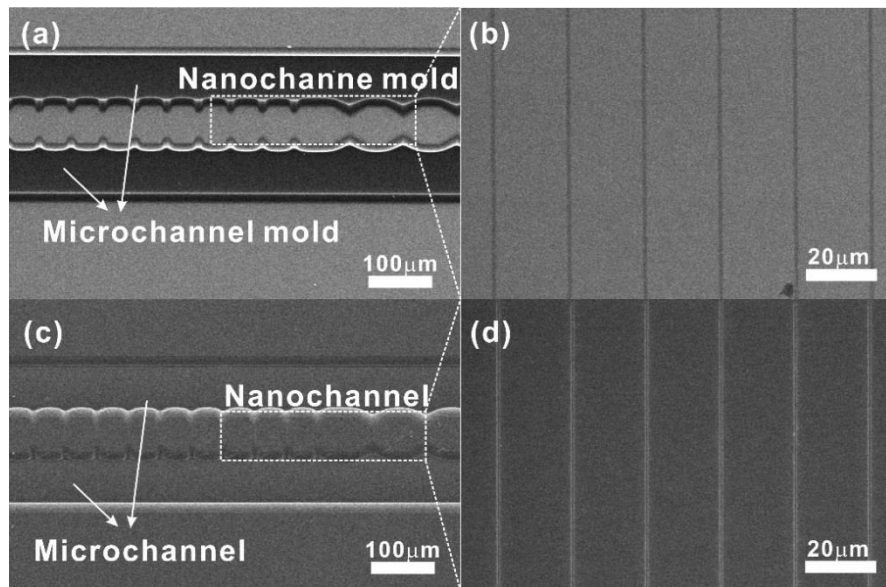
Figure 3.5 (a) SEM image of mixed-scale carbon mold and (b) magnified nanochannel carbon mold image. (c) Corresponding SEM images of PMMA mixed-channel networks transferred by thermal nanoimprint and (d) magnified nanochannel image. PMMA mixed-scale channels were accurately transferred from mixed-scale convex carbon mold.
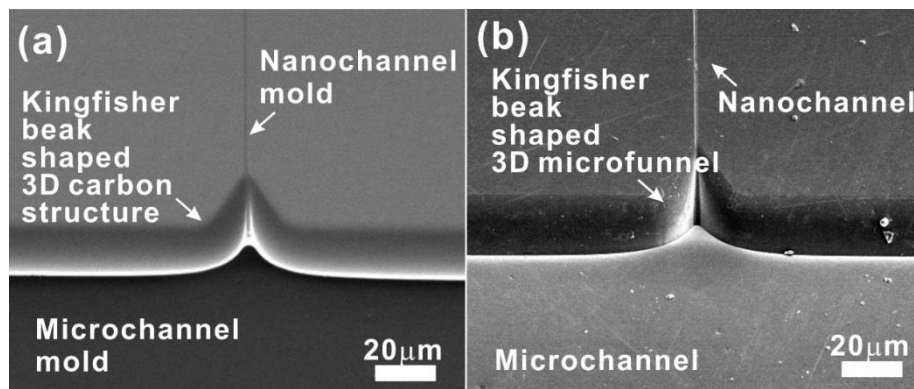
Figure 3.6 SEM images of (a) micro- and nanochannel mold with Kingfisher-beak-shaped 3D carbon structure and (b) corresponded PMMA micro- and nanochannel with Kingfisher-beak-shaped 3D microfunnel. This 3D microfunnel connects microchannel and nanochannel smoothly via gradually reduced cross section.

3.2.2 Characterization of nanochannel fabrication

The morphology change of small-scale SU-8 into carbon nanochannel mold and transferred PMMA channel pattern are shown in figure 3.6. Figure 3.7 (a) – (c) are SEM images and figure 3.7 (d) – (f) are AFM (atomic force microscopy) images. Figure 3.8 shows profile of cross section of small-scale SU-8, carbon nanochannel mold, and transferred PMMA nanochannels measured by AFM. The reduction of width and change of vertical side wall can be seen. After nanoimprint process, nanochannel pattern was engraved on the PMMA surface and width of nanochannel was similar with carbon nanochannel mold width.

The actual decrease of width and height is shown in figure 3.7 and 3.8. After pyrolysis, 1 μm-width and 420 nm-height SU-8 structure was changed into 1 μm (bottom)/ 600 nm (top)-width and 60 nm-height shrunk carbon mold. The total shrinkage was ~ 85 % in height. After nanoimprint, nanochannel transferred accurately comparing with carbon mold. The width and depth of nanochannel was almost 600 nm and ~ 60 nm, respectively. Totally, the size of the large and small-scale SU-8 structure, shrunk micro and nano carbon structure, and transferred PMMA micro and nanochannel pattern are described in table 3.2.

		SU-8	Carbon mold	PMMA channel
Nanoscale	Width	1 μm	1 μm (bottom) ~ 600 nm (top)	600 nm
	Height / Depth	420 nm	63 - 67 nm	60 - 65 nm
Microscale	Width	100 μm	100 μm (bottom) ~ 50 μm (top)	~ 50 μm
	Height / Depth	25 μm	5 ~ 6 μm	5~ 6 μm

Table 3.2. The measured value of SU-8, carbon, and PMMA in width and height/depth.
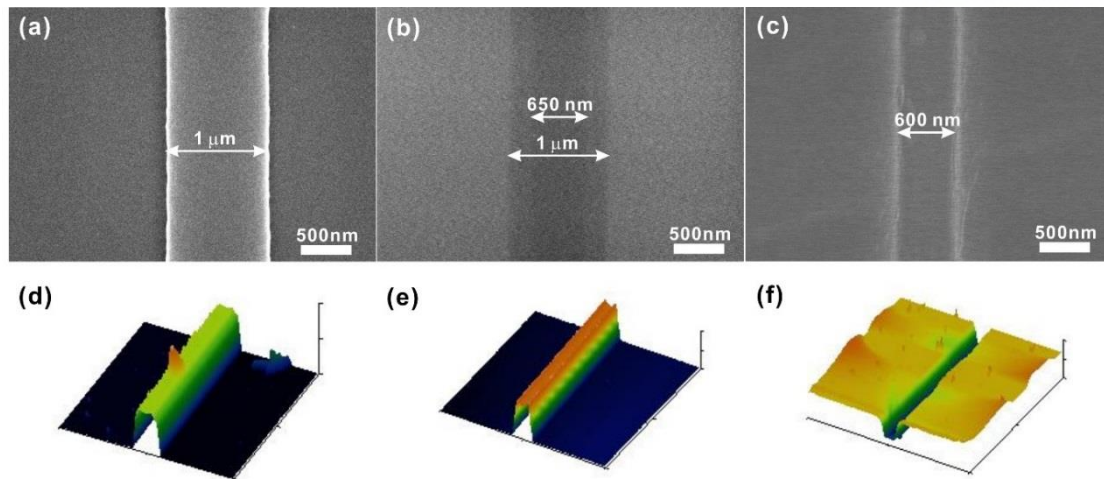
Figure 3.7 SEM images of (a) small-scale SU-8, (b) pyrolyzed nanochannel carbon mold, and (c) PMMA nanochannel pattern. 1 μm SU-8 small-scale precursor width was reduced to ~ 600 nm in carbon and corresponded nanochannel width is almost 600 nm. The height or depth of (a) small-scale SU-8, (b) pyrolyzed nanochannel carbon mold, and (f) PMMA nanochannel were measured by atomic force microscope (AFM).
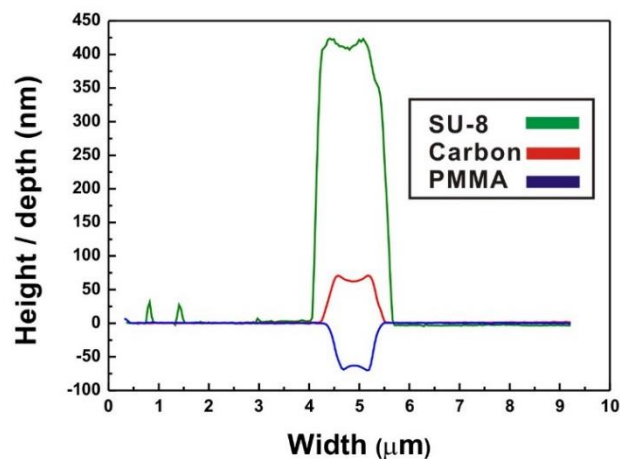
Figure 3.8 AFM measurement of cross section profile of smalls scale SU-8 structure, carbon nanochannel mold, and PMMA nanochannel. 420 nm-height SU-8 was decreased into ~ 60 nm-height carbon structure and which was engraved 60 nm depth channels on the PMMA.

3.2.3 Sealing test of mixed-scale channel networks

After oxygen plasma treatment, channel transferred PMMA sheet and a 175 μm-thick PMMA sheet were bonded at 75 °C with 0.2 MPa pressure. The completed PMMA fluidic device filled with green colored solution (Fig. 3.9 (a)). To check the channel sealing completeness, 1 mM FITC solution

43

(Fluorescein sodium salt (Sigma Aldrich, Korea) dissolved in DI water) was filled in the PMMA mixed-scale channels (Fig. 3.9 (b) - (e)) and took images by inverted microscope and SEM. Since the channel maintained hydrophilicity after thermal bonding, solution flowed inside PMMA channel naturally. From figure 3.9 (b), it was demonstrated that nanochannels were clearly sealed and there was not channel collapse or channel leakage comparing with the corresponding SEM image of nanochannel (Fig. 3.9 (c)). Figure 3.9 (d) and (e) show mixed-scale channels were well connected via 3D microfunnels. Those images were taken by confocal inverted microscope in UOBC (Multi-photon confocal microscopy, LSM 780 configuration 16 NLO, Carl Zeiss).
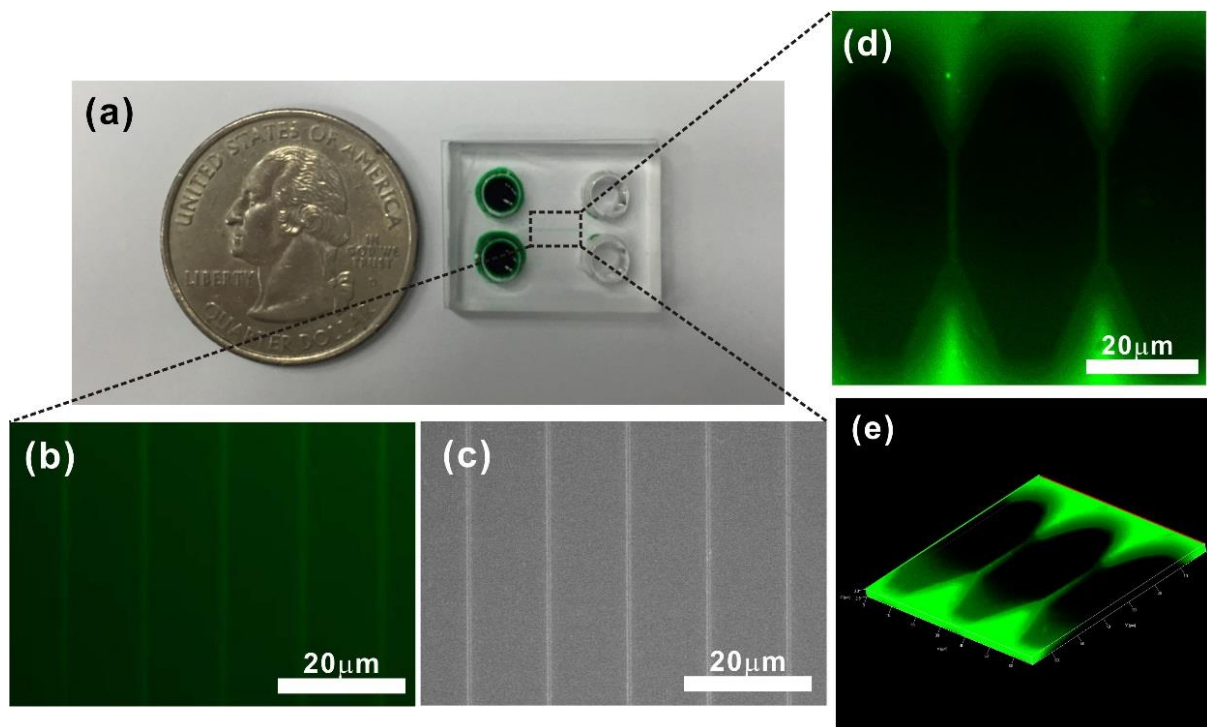
Figure 3.9 (a) Completed mixed-scale fluidic device after oxygen plasma assisted thermal bonding comparing with a 25 cents coin. (b) Inverted microscope image of nanochannels filled with 1mM FITC solution without channel collapse. (c) SEM image of corresponding nanochannels. (d) 2D and (e) 3D confocal microscope image of nanochannels with 3D microfunnels filled with 1mM FITC solution.

4

Application

The completed mixed-scale fluidic device is used

to single particle entrapment

via diffusiophoresis.

4. Application of single particle entrapment in Kingfisher-beak-shaped 3D microfunnels via diffusiohoresis

4.1 Necessity

Generally, biomolecule study is necessary for biomedical research, for which, micro/nanofluidics or mixed-scale fluidic device is generally used as a bioanalysis tool which are called lab on a chip. Before analyzing biomolecules, analyzed samples such as DNA or cells are delivered in specific location where samples are placed and confined. However, the small biomolecule delivery is difficult, so those materials were dragged by electrical force in previous researches since those generally have electrical charge. Representatively, DNA molecule having negative charge is drawn via electric fields so DNA can pass through narrow nanochannel in being uncoiled which makes DNA sequencing. However, electric field is limitedly utilized in molecules manipulation having electrical charge only and it is imposed in wide range reservoir and channels so many particles are moved all together not individually. In addition, weakly charged or un-charged particles need strong electric fields or other methods.

Recently, individual particle delivery has been required for single cell study. In this case, the cells are delivered individually in a micro chamber for being confined to be analyzed. By injecting drugs or gens through nanochannel to the single cell, the response of single cell can be observed. This method is called nanoelectroporation and have been paid attention since it has high cell viability and effective controllability of injection of drugs or gene. But the problem is how to deliver individual cell in a single chamber separately. To achieve it, novel single cell driving force need to be suggested with structurally

appropriate single cell chamber.

In previous research, Kingfisher-beak-shaped 3D microfunnel was successfully utilized as a single particle chamber and the particles were dragged by electrical force one by one. Even though the effectiveness of the unique 3D microfunnel structure was demonstrated, too much strong electric field and result of randomly trapped particles should be replenished. The strong electric field tightly entrapped particles which may lead to cell damage in real bioengineering research and result of random entrapment means low efficiency of the manipulation method. Here, we try to use Kingfisher-beak-shaped 3D microfunnel structure for single particle entrapment via diffusiophoresis method. From this research, the usefulness of Kingfisher-beak-shaped 3D microfunnel in terms of diffusiophoresis and single particle chamber can be demonstrated. In addition, we suggest the diffusiophoresis as a novel and effective particle delivery method for various single cell studies.

4.2 Diffusiophoresis

In concentration gradient of solute existing region, colloidal particles are driven without any external forces. This phenomenon is called diffusiophoresis and it leads spontaneous particles movement because the chemical energy is changed into the mechanical energy [50 – 52]. So, it is generally used in a migration of colloidal particles dispersed in solution. The mechanical energy consists of two kinds of driving force; electrophoresis and chemiphoresis.

First, electrophoresis of a particle is caused by spontaneously formed electric field in a solute concentration gradient region. The difference of diffusion coefficient between anions and cations

develops local electric field, some particles having zeta potential are easily attracted due to the electric

field (E).

$$E = \frac{kT}{Ze}\frac{D_+ - D_-}{D_+ + D_-}\frac{\nabla n}{n} \quad [52]$$

Here, k is Boltzmann's constant, T is temperature, e is proton charge, Z is the valence of a

symmetric Z:Z electrolyte, n is the local salt concentration, and D_+ and D_- are the diffusion

coefficients of the cation and the anion, respectively. The magnitude of this electric field depends on

the difference of diffusion coefficients of the ions and the length over which the gradient is set up.

Second, chemiphoresis of a particle is caused by osmotic pressure gradient within a narrow interaction

region above the particle surface. Because of the pressure gradient within particle surface, opposite

propulsion is emerged so particles can be moved. These two types of forces are summarized in particles,

which conclude particle moving direction, velocity, and movement tendency. However, for

completeness, chemiphoresis effect can be ignored since the chemiphoresis less influences to transport

rates [52].
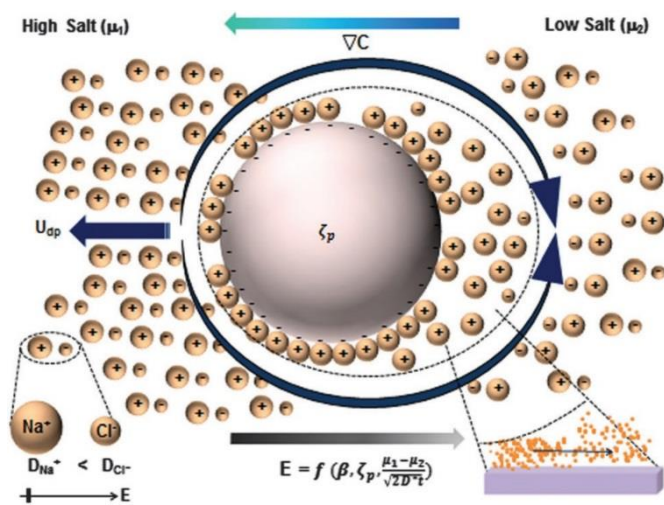
Figure 4.1 Essential mechanism of electrolyte diffusiophoresis. The mechanism consists of two parallel additive phenomena: electrophoresis and chemiphoresis [53].

As one of advanced application of diffusiophoresis, we used this phenomenon as a driving force for single particle entrapment. In fact, diffusiophoresis was only used in particle colloids because it is difficult to localize solute gradient region in specific location. In this paper, we utilize the unique structure of Kingfisher-beak-shaped 3D microfunnel structure for localizing solute gradient. By this way, single particles are entrapped in the 3D microfunnel, one by one. This is the first time to show the possibility of diffusiophoresis as a single particle entrapment driving source.
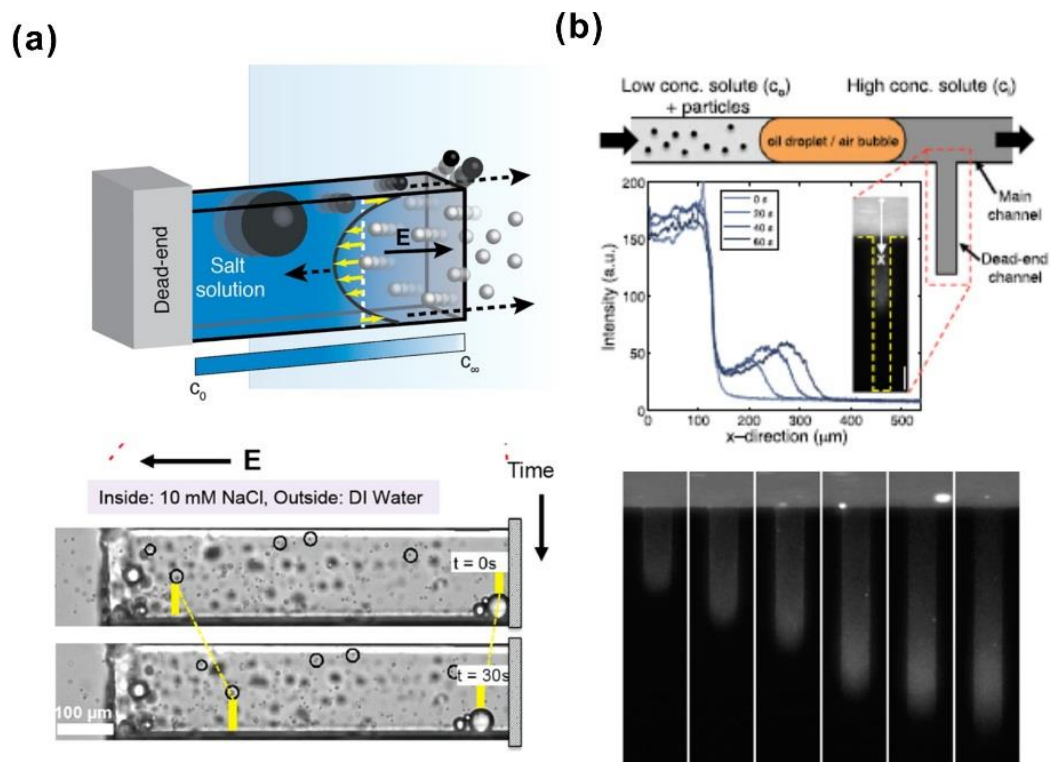
Figure 4.2 Colloidal particle movement in dead-end channel via diffusiophoreisis. (a) Enhanced transport into and out of dead-end pores from Kar et al. [52] and (b) size-dependent control of colloid transport from Shin et al. [51].

4.3 Experiment

As described in figure 4.3, we can localize solute gradient region in Kingfisher-beak-shaped 3D microfunnels clearly fabricated by mixed-scale carbon mold and nanoimprint process.

First, filled 2 mM NaCl solution in bottom microchannel through two bottom reservoirs. And 0.02 mM NaCl solution with 1 μm-diameter polycarboxylate microparticles (Polyscience Inc.) dispersed (1 wt%) was filled in top and left side of reservoir. Then, 0.02 mM NaCl with 1 μm-diameter polycarboxylate microparticles were flowing from left to right through microchannel. By filling 0.02 mM NaCl solution without particles in top and right side reservoir, controlled particle flowing speed. The difference of hydraulic pressure between top and bottom microchannels, 2 mM NaCl solution were flowing from microchannels to 3D microfunnels through nanochannels. And 0.02 mM NaCl solution were flowing continuously through microchannels so the edge of microfunnels were consistently washed by low concentrate solution, therefore, in 3D microfunnels, consistent solute gradient region could be fabricated. This consequently resulted in spontaneous electric field via diffusion coefficient difference of Na and Cl and attracted single particle into 3D microfunnel, one by one.
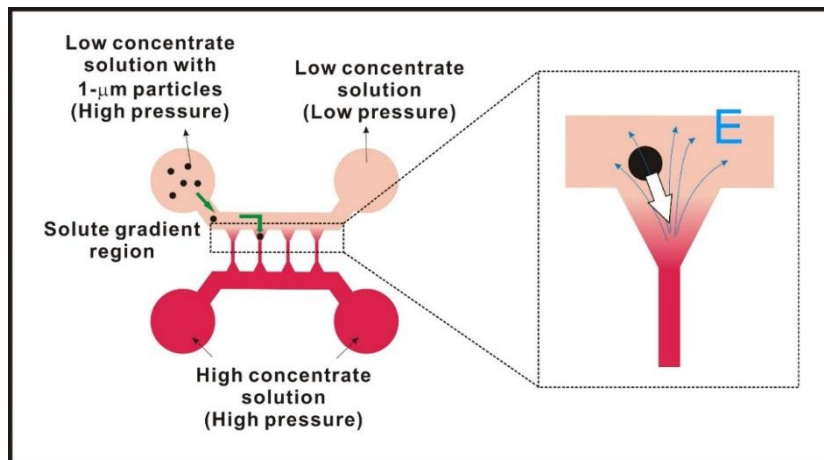
Figure 4.3 Schematic of experiment method how to localize solute gradient region in 3D microfunnel and process of particle entrapment via localized electric field.

4.4 Results

As demonstrated in figure 4.4, single particles were successfully entrapped in 3D microfunnel

within 5 minutes. This experiment is high reproducible and has good possibility of success. From this

result, diffusiophoresis can be suggested to be utilized not only for colloid particle movement but also

single particle entrapment for single cell study.

When 8 mM NaCl solution was used instead of 2 mM NaCl solution, plenty of particles were

dragged in 3D microfunnels simultaneously (Fig. 4.5 (a)). Because the spontaneous diffusiophoresis

effect was too strong so many particles were affected at the same time. The similar result of several

particle entrapment phenomenon could be seen in the first experiment case after 30min (Fig. 4.5 (b)).

After single particles were entrapped, other additional particles were entrapped in 3D microfunnel

where one particle had been trapped (Fig. 4.5 (b)). This was because particle couldn't block inlet of 3D

microfunnel connected to nanochannel certainly, therefore, there remains solute gradient which cause

diffusiophoresis. For trapping single particle only, NaCl concentration should be optimized to control

strength of driving force.

Depending on the presence of 3D microfunnel, particle entrapment efficiency could be changed

described in figure 4.6. If there was not 3D microfunnel, microchannels and nanochannel were

connected directly (Fig. 4.6 (b)). In this case, a lot of particles were just attracted near nanochannels but

not to be stick to specific points. Similarly, in case of figure 4.6 (c), 2 and half microfunnel structures

were placed between microchannels and nanochannels. But particles were just attracted near

nanochannels.

As a result, it was demonstrated that Kingfisher-beak-shaped 3D microfunnels is effective structure as a chamber and beneficial structure for localizing solute gradient region. This result can be compared with 2 and half microfunnel and no funnel structure where no single particle was entrapped and the particles were just attracted near diffusiophoresis affected region. So, the attracted particles were not confined and flowed with low concentrate solution flowing in microchannel.
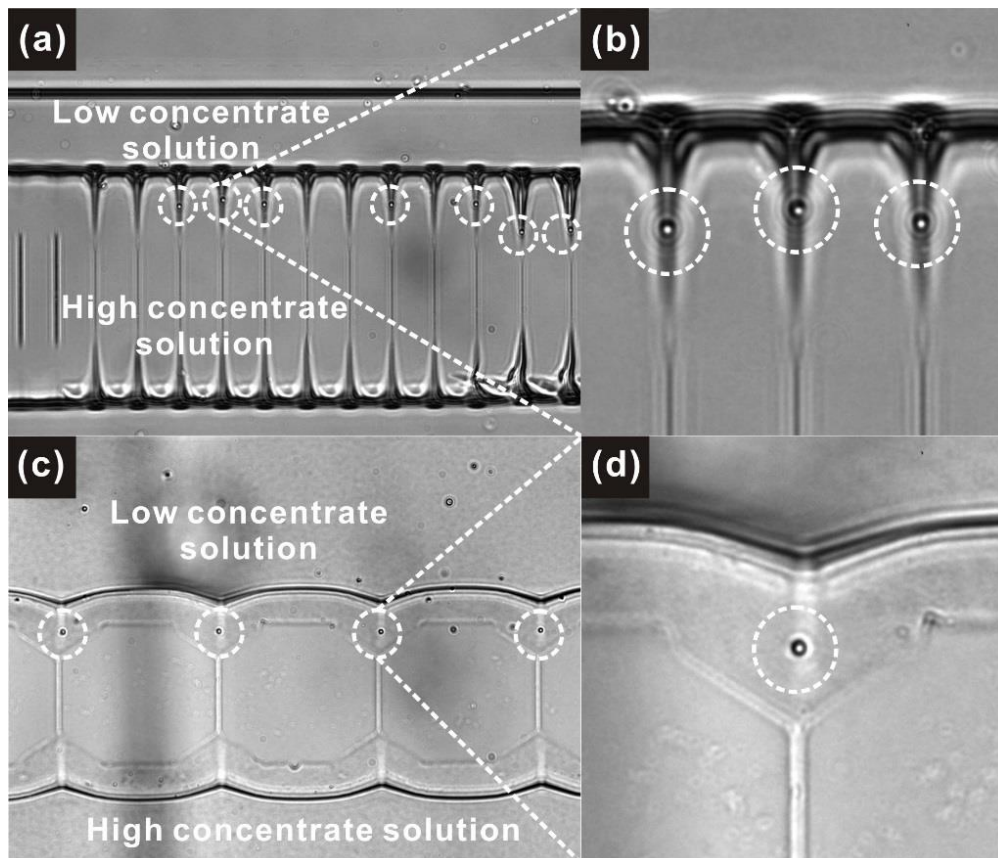
Figure 4.4 Inverted microscope images of single particle entrapment in 3D microfunnel within 5 minutes. (a) Single particle entrapment in narrow funnel with (b) corresponding enlarged image and (c) single particle entrapment in wide funnel with (d) corresponding enlarged image.
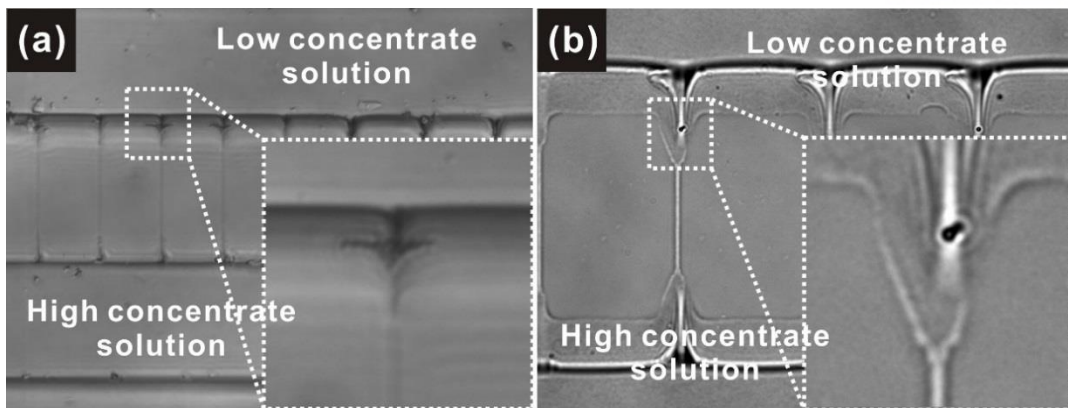
Figure 4.5 Inverted microscope images of multiple particles entrapment. (a) In case of using 8 mM high concentrate NaCl solution, several particles are simultaneously attracted in 3D microfunnel. (b) In the same case in figure 4.4, some additional particles were dragged in 3D microfunnel after 30 min single particle entrapment.
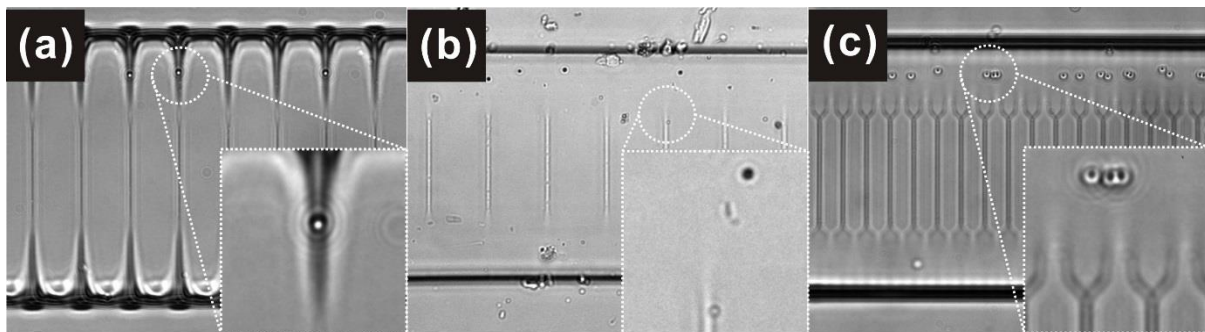
Figure 4.6 Inverted microscope images of particle entrapment in (a) 3D microfunnel, (b) no funnel, and (c) 2D and half microfunnel. Comparing with (a), there was no particle entrapment in (b) and (c), just the particles were attracted near nanochannels where solute gradient existed.

5

Conclusion

In this chapter, the conclusion of this thesis is stated.

5. Conclusion

In this research, the fabrication of mixed-scale PMMA fluidic device was developed via thermal nanoimprint using a monolithic mixed-scale convex carbon mold. Using carbon-MEMS technique, a monolithic convex mixed-scale carbon structure was fabricated by two step photolithography and a pyrolysis processes. Owing to the large volume reduction during pyrolysis, the microscale photoresist polymer structure (large-scale polymer: 25 µm-height and 100 µm-width, small-scale polymer: 420 nm-height and 1 µm-width) could be changed into carbon structure at the sub-micro/nanoscale (microscale carbon: 5 µm-height and 50 µm- width, nanoscale carbon: 60 nm-height and 600 nm-width) without using nanofabrication methods such as e-beam lithography and focused ion beam milling. The pyrolyzed carbon had high Young's modulus and hardness (Young's modulus: 28 GPa, hardness: 3.67 GPa) so that it could transfer channel patterns on PMMA sheets. more than 40 times. PMMA has relatively high Young's modulus and hardness comparing to PDMS and thus collapse-free nanochannel fabrication was enabled. This novel fabrication process overcomes the disadvantages of pre-existing nanofabrication methods such as low throughput, complexity, high cost, and nanochannel collapse issue.

This PMMA mixed-scale fluidic device enabled single particle entrapment using diffusiophoresis at Kingfisher-beak-shaped 3D microfunnels because of their characteristic 3D architecture. This result showed the applicability of the PMMA mixed-scale fluidic device with 3D microfunnel for the wide range of research areas such as single cell study and nanoelectroporation.

References

[1] Sung Jae Kim, Yong-Ak Song, and Jongyoon Han, "Nanofluidic concentration devices for biomolecules utilizing ion concentration polarization: theory, fabrication, applications", *Chem. Soc. Rev.*, **39**, 912-922 (2010).

[2] Bumjoo Kim, Joonseong Heo, Hyukjin J. Kwon, Seong J. Cho, Jongyoon Han, Sung Jae Kim, and Geunbae Lim, "Tunable ionic transport for a triangular nanochannel in a polymeric nanofluidic system", *ACS Nano*, **7**, 740-747 (2013).

[3] H. Daiguiji, "Ion transport in nanofluidic channels", *Chem. Soc. Rev.*, **39**, 901-911 (2010).

[4] Nicholas Douville, Dongeun Huh, Shuichi Takayama, "DNA linearization through confinement in nanofluidic channels", *Anal. Bioanal. Chem.*, **391**, 2395-2409 (2008).

[5] Rohit Karnik, Chuanhua Duan, Kenneth Castelino, Hirofumi Daiguji, and Arun Majumdar, "Rectification of ion current in a nanofluidic diode", *Nano Lett.*, **7**, 547-551 (2007).

[6] Cheng, L. J. and Guo, L. J., "Ion current rectification, breakdown, and switching in heterogeneous oxide nanofluidic devices", *ACS Nano*, **3**, 575-584 (2009).

[7] Pan Mao and Jongyoon Han, "Massively-parallel ultra-high-aspect-ratio nanochannels as mesoporous membranes", *Lab chip*, **9**, 586-591 (2009).

[8] Sangmin Lee, Min Park, Heon-Seok Park, Yeongae Kim, Siwoo Cho, Jae Hyoung Cho, Jaesung Park and Woonbong Hwang, "A polyethylene oxide-functionalized self-organized alumina nanochannel array for an immunoprotection biofilter", *Lab chip,* **11**, 1049-1053 (2011).

[9] Keliang Gao, Lei L, Lingna HE, Kevin Hinkle, Yun Wu, Junyu Ma, Lingqian Chang, Xi Zhao, Daniel Gallego Perez, Sigrid Eckardt, John Mclaughlin, Boyu Liu, Dave F. Farson, and L. James Lee, "Design of a microchannel-nanochannel-microchannel array based nanoelectroporation system for precise gene transfection", *Small,* **5**, 1015-1023 (2014).

[10] Sung Jae Kim, Sung Hee Ko, Kwang Hyoung Kang, Jongyoon Han, "Direct seawater desalination by ion concentration polarization", *Nat. Nanotech.*, **5**, 297-301 (2010).

[11] Ying-Chih Wang and Jongyoon Han, "Pre-binding dynamic range and sensitivity enhancement for immune-sensors using nanofluidic preconcentrator", *Lab chip*, **8**, 392-394 (2008).

[12] Laurent D. Menard, Chad E. Mair, Michael E. Woodson, Jean Pierre Alarie, and J. Michael Ramsey, "A device for performing lateral conductance measurements on individual double-stranded DNA molecules", *ACS Nano*, **10**, 9087-9094 (2012).

[13] Seung-min Park, Yun Suk Huh, Kylan Szeto, Daniel J. Joe, Jun Kameoka, Geoffrey W. Coates, Joshua B. Edel, David Erickson, and Harold G. Craighead, "Rapid prototyping of nanofluidic systems using size-reduced electrospun nanofibers for biomolecular analysis" *Small*, **6**, 2420-2426 (2010).

[14] Welhua Guan, Rong Fan, and Mark A. Reed, "Field-effect reconfigurable nanofluidic ionic diodes" *Nat. Comm.,* **2**, 506(8) (2011).

[15] Noritada Kaji, Yojiro Tezuka, Yuzuru Takamura, Masanori Ueda, Takahiro Nishimoto, Hiroaki Nakanishi, Yasuhiro Horiike, and Yoshinobu Baba, "Separation of long DNA molecules by quartz nanopillar chips under a direct current electric field", *Anal. Chem*., **76**, 15-22 (2004).

[16] Michelle L. Kovarik and Stephen C. Jacobson, "Integrated nanopore/microchannel devices for an electrokinetic trapping of particles", *Anal. Chem*., **80**, 657-664 (2008).

[17] Yunjeong Lee, Yeongjin Lim and Heungjoo Shin, "Mixed-scale channel networks infludic kingfisher-beak-shaped 3D microfunnels for efficient single particle entrapment", *Nanoscale*, **8**, 11810-11817 (2016).

[18] Pouyan E. Boukany, Andrew MNorss, Wei-ching Liao, Brian Henslee, Hyunchul Jung, Xulang Zhang, Bo Yu, Xinmei Wang, Yun Wu, Lei Le, Keliang Gao, Xin Hu, Xi Zhao, O. Hemminger, Wu Lu, Gregory P. Lafyatis and L James Lee, "Nanochannel electroporation delivers precise amounts of biomolecules into living cells", *Nat. Nanotech.,* **6**, 747-754 (2011).

[19] Xi Zhao, Xiaomeng Huang, Xinmei Wang, Yun Wu, Ann-Kathrin Eisfeld, Sebastian Schwind, Daniel Gallego-Perez, Pouyan E. Boukany, Guido I. Marcucci, and Ly James Lee, "Nanochannel electroporation as a plaform for living cell interrogation in acute myeloid leukemia", *Adv. Sci*., **2**, 1500111(5) (2015).

[20] Michelle L. Kovarik and Stephen C. Jacobson, "Nanofluidics in lab-on-a-chip devices", *Anal. Chem*., **82**, 7133-7140 (2009).

[21] Dogyeong Ha, Jisoo Hong, Heungjoo Shin, and Taesung Kim, "Unconventional micro-/nanofabrication technologies for hybrid-scale lab-on-a-chip", *Lab chip*, **16**, 4296-4312 (2016).

[22] Z. Xu, J. K. Wen, C. Liu, J. S. Liu, L. Q. Du and L. D. Wang, "Research on forming and application of U-form glass micro-nanofluidic chip with long nanochannels", *Microfluid. Nanofluid.*, **7**, 423-429 (2009).

[23] D. W. Inglis, E. M. Goldys and N. P. Calander, "Simultaneous concentration and separation of proteins in a nanochannel", *Angew. Chem., Int. Ed.*, **50**, 7546-7555 (2011).

[24] K. Aizel, V. Agache, C. Pudda, F. Bottausci, C. Fraisseix, J. Bruniaux, F. Navarro and Y. Fouillet, "Enrichment of nanoparticles and bacteria using electroless and manual actuation modes of a bypass nanofluidic device", *Lab chip*, **13**, 4476-4485 (2013).

[25] Walter Reisner, Niels B. Larsen, Asli Silahtaroglu, Anders Kristensen, Niels Tommerup, Jonas O. Tegenfeldt, and Henrik Flyvbjerg, "Single-molecule denaturation mapping of DNA in nanofluidic channels", *PNAS,* **107**,13294-13299 (2010**).**

[26] John M. Perry, Zachary D. Harms, Stephen C. Jacobson, "3D nanofluidic channels shaped by electron-beam-induced etching", *Small*, **8**, 1521-1526 (2012).

[27] T. Yasui, N. Kaji, R. Ogawa, S. Hashioka, M. Tokeshi, Y. Horiike and Y. Baba, "DNA separation in nanowall array chips", *Anal. Chem.*, **83**, 6653-6640 (2011).

[28] E. Angeli, A. Volpe, P. Fanzio, L. Repetto, G. Firpo, P. Guida, R. Lo Savio, M. Wanunu and U. Valbusa, "Simultaneous electro-optical tracking for nanoparticle recognition and counting" *Nano Lett.*, **15**, 5696-5701 (2015).

[29] E. Angeli, C. Manneschi, L. Repetto, G. Firpo and U. Valbusa, "DNA manipulation with elastomeric nanostructures fabricated by soft-moulding of a FIB-patterned stamp", *Lab chip*, **11**, 2625-2629 (2011).

[30] Laurent D. Menard and J. Michael Ramsey, "Electrokinetically-driven transport of DNA through focused ion beam milled nanofluidic channels", *Anal. Chem.*, **85**, 1146-1153 (2013).

[31] Xi Zhao, Yun Wu, Daniel Gallego-Perez, Kwang Joo Kwak, Cherry Gupta, Xilian Ouyang, and Ly James Lee, "Effect of nonendocytic uptake of nanoparticles on human bronchial epithelial cells", *Anal. Chem*, **87**, 3208-3215 (2015).

[32] Huan Hu, Yue Zhuo, Muhammed E Oruc, Brian T Cunningham and Willian P King, "Nanofluidic channels for arbitrary shapes fabricated by tip-based nanofabrication", *Nanotechnology*, **25**, 455301

(8pp) (2014).

[33] Fan Liu, Kheng Boon Tan, P. Malar, S.K. Bikkarolla, J.A. van Kan, "Fabrication of nickel molds using proton beam writing for micro/nano fluidic devices", *Microelectronic Engineering*, **102**, 36-39 (2013).

[34] Gaku Isobe, Isaku Kanno, Hidetoshi Kotera, Ryuji Yokokawa, "Perfusable multi-scale channels fabricated by integration of nanoimprint lithography (NIL) and UV lithography (UVL)", *Microelectronic Engineering*, **98**, 58-63 (2012).

[35] Paola Fanzio, Valentina Mussi, Chiara Manneschi, Elena Angeli, Giuseppe Firpo, Luca Repetto, and Ugo Valbusa, "DNA detection with a polymeric nanochannel device", *Lab chip*, **11**, 2961-2966 (2011).

[36] Zhifu Yin, Lei Sun, Helin Zou and E Cheng, "Two dimensional PMMA nanofluidic device fabricated by hot embossing and oxygen plasma assisted thermal bonding methods", *Nanotechnology*, **26**, 215302 (12pp) (2015).

[37] Franklin I. Uba, Bo Hu, Kumuditha Weerakoon-Ratnayake, Nyote Oliver-Calixte and Steven A. Soper, "High process yield rates of thermoplastic nanofluidic devices using a hybrid thermal assembly technique", *Lab chip*, **15**, 1038-1049 (2015).

[38] Zhifu Yin, E Cheng and Helin Zou, "A novel hybrid patterning technique for micro and nanochannel fabrication by integrating hot embossing and inverse UV photolithography", *Lab chip*, **14**, 1614-1621 (2014).

[39] E. Abad, A. Juarros, A. Retolaza, S. Merino, R. Marie, A. Kristensen, "DNA analysis by single molecule stretching in nanofluidic biochips", *Microelectronic Engineering*, **88**, 300-304 (2011).

[40] Y. H. Cho, J. Park, H. Park, X. Cheng, B. J. Kim, A. Han, "Fabrication of high-aspect-ratio polymer nanochannels using a novel Si nanoimprint mold and solvent-assisted sealing", *Microfluid Nanofluid*, **9**, 163-170 (2010).

[41] C. Wang, L. Taherabadi, G. Jia, M. Madou, Y. Yeh and B. Dunn, "C-MEMS for the manufacture of 3D microbatteries", *Electrochemical and Solid-State Letters*, **7**, A435-A438 (2004).

[42] J. Heo, D. Shim, G. T. Teixidor, S. Oh, M. Madou and H. Shin, "Carbon interdigitated array nanoelectrodes for electrochemical applications", *Journal of the Electrochemical Society*, **158,** J76-J80 (2011).

[43] Y. Lim, J.-I. Heo, M. Madou and H. Shin, "Monolithic carbon structures including suspended single nanowires and nanomeshes as a sensor platform", *Nanoscale research letters*, **8**, 1-9 (2013).

[44] Y. Lim, J.-I. Heo and H. Shin, "Fabrication and application of a stacked carbon electrode set including a suspended mesh made of nanowires and a substrate-bound planar electrode toward for an electrochemical/biosensor platform", *Sensors and Actuators B: Chemical*, **192**, 796-803 (2014).

[45] S.-W. Youn, A. Ueno, M. Takahashi and R. Maeda, "A process of glassy carbon etching without the micro masking effect for the fabrication of a mold with a high-quality surface", *Journal of Micromechanics and Microengineering*, **19**, 125010 (2009).

[46] S. W. Youn, M. Takahashi, H. Goto and R. Maeda, "A study on focused ion beam milling of glassy carbon molds for the thermal imprinting of quartz and borosilicate glasses", *Journal of Micromechanics and Microengineering*, **16**, 2576 (2006).

[47] J. Ju, S. Lim, J. Seok and S.-m. Kim, "A method to fabricate Low-Cost and large area vitreous carbon mold for glass molded microstructures", *International Journal of Precision Engineering and Manufacturing*, **16**, 287-291 (2015).

[48] Jiahao Wu, Rattikan Chantiwas, Alborz Amirsadeghi, Steven A. Soper and Sunggook Park, "Complete plastic nanofluidic devices for DNA analysis via direct imprinting with polymer stamps", *Lab chip*, **11**, 2984-29889 (2011).

[49] Rattikan Chantiwas, Mateusz L. Hupert, Swathi R. Pullagurla, Subramanian Balamurugan, Jesus Tamarit-Lopez, Sunggook Park, Proyag Datta, Jost Goettert, Yoon-Kyoung Cho and Steven A. Soper, "Simple replication methods for producing nanoslits in thermoplastics and the transport dynamics of double-stranded DNA through these slits", *Lab chip*, **10,** 3255-3264 (2010).

[50] J. P. Ebel, J. L. Anderson, and D. C. Prieve, "Diffusiophoresis of latex particles in electrolyte gradients", Langmuir, 4, 396-406 (1988)/

[51] Sangwoo Shin, Eujin Um, Benedikt Sabass, Jesse T. Ault, Mohammad Rahimi, Patrick B. Warren, and Howard A. Ston, "Size-dependent control of colloid transport via solute gradient in dead-end channels", *PNAS*, **13**, 257-261 (2016).

[52] Abhishek Kar, Tso-Yi Chiang, Isamar Oritz Rivera, Ayusma Sen, and Darrel Velego, "Enhanced transport into and out of dead-end pores" *ACS nano*, **9**, 746-753 (2015).

[53] Darrel Velegol, Astha Garg, Rajarshi Guha, Abhishek Kar and Manish Kumar, "Origins of concentration gradients for diffusiophoresis", *Soft Matter*, **12**, 4686-4703 (2016).

Acknowledgements

I deeply thanks to my advisor, Professor Heungjoo Shin. He always inspired me to improve my research work with a kindness and wisdom. He was a great teacher in study and good advisor of my life. Without his guidance and supports, I couldn't finish this thesis. I take this opportunity to say the appreciation of his helps. I also appreciate to the committee members, Professor Taesung Kim and Professor Hoon Eui Jeong for giving their wise words, suggestion and assistance during the preparation with this thesis. Thanks to them, I could successfully complete this thesis.

And I want to give my thanks to all MNIS Lab Members. Owing to their helps, I could finish my master course and spent happy and joyful time in Ulsan. Specially, I also want to say thank to Microfluidics/ Nanomechatronics (μFNM) Lab members who gave me countless helps and advices for experiment and allowed me to use their equipment many times. Above them, I extend to express the thanks to the female members of mechanical engineering including Sangan Park, Jiyun Jeon, Inseong Jo and Hyunha Park. Owing to all my colleagues, I could spend unforgettable 2 years. I'll never forget the memory in UNIST.

Whenever I was depressed, my family always trusted me and gave infinite love. Owing to their dedication, I got every confidence from my father, sweet and gentle love from my mother, courage from my older sister and great concerns from my aunts, uncles, and cousins. I sincerely appreciate to them. Specially, I want to say thank you to J-Sik for his warm hearts. Finally, I want to give thanks to him for his kindness and endless love. I'll always keep his words and make a good work.